FULL LENGTH ARTICLE

Eleyon NANOSCALE REPORTS

DOI: 10.26524/nr1814

Highlighted Article

Visible photocatalytic activity of metal ion doped and undoped nano ZnO for the degradation of Acidal Navy Blue 3BR

G. Thennarasu [a,*], A. Sivasamy [b,*]

[a] Department of Chemistry, C. Kandaswami Naidu College for Men, Unit of Pachaiyappa's Trust,Chennai-600 102, Tamil Nadu, India

[b] Chemical Engineering Department, CSIR- Central Leather Research Institute, Adyar, Chennai-600 020, Tamil Nadu, India

***Corresponding Author**
sivasamy@clri.res.in
(A. Sivasamy)

Tel.: +91

Received : 30-01-2018
Accepted : 13-02-2018

ABSTRACT: Metal (Mn, Cu, Co) doped and undoped Nano ZnO, prepared by chemical precipitation method and calcined at 300°C was characterized by XRD, FE-SEM, FT-IR, DRS and TEM. These photo catalysts can be effectively degrade organic contaminants using visible light irradiation. Doping reduces the intra granular resistance and recombination of the photo generated electron–hole pairs. The photo activity of undoped and doped ZnO powders was evaluated by monitoring the photo-decolourization of the aqueous solutions of Acidal Navy Blue 3BR (ANB 3BR) dye under visible irradiation. The disappearance of dye molecules followed pseudo-first-order kinetics. The effect of various parameters namely, pH of the medium, catalyst loading, initial dye concentration and kinetics of photo degradation of ANB 3BR was investigated. The rate of degradation was found to be strongly influenced by all above mentioned parameters. The reduction in the chemical oxygen demand (COD) of the decolorized aqueous samples revealed a possibility of complete destruction of the organic molecules along with colour removal. Experimental data were analyzed by model equations such as Langmuir and Freundlich isotherms and it was found that the Langmuir isotherm model best fitted the adsorption data. The results showed that the doped (Mn, Cu, Co) percentage (0.25, 0.5, 0.75, 1, 1.5%) were successfully doped into the ZnO and that manganese and copper-doping reduced the photo catalytic activity of ZnO, Co doped ZnO increase the photo catalytic activity.1%, 0.75%, 0.75% of Mn, Cu, Co doped in ZnO can be used in photo catalytic experiments.
.

Keywords: Visible light, ZnO, photo catalysis, doping, synthesis

1 Introduction

Photo catalytic degradation of organic compounds for the purpose of purifying dye Wastewater from industries and households has attracted much attention in recent years [1-5]. The industrial importance of ZnO as a UV blocking agent, experiments involving the reduction of the photo catalysis of ZnO have scarcely been reported [6]. One approach to eliminate the photo catalytic activity is to dope ZnO with impurity ions. It is generally considered that doping ions create defects in the crystal lattice that act as trapping sites of the excitants, promoting recombination of electron-hole pairs, resulting in reduced photo catalytic activity [7]. For example, the doping of manganese ions in ZnO creates deep traps within the band gap, which may act as electron-hole recombination sites [8]. The application of semiconductors such as ZnO and TiO_2 in the area of photo catalysis has grown considerably, primarily because of their physical and chemical stability, high oxidative capacity, low cost and ease of availability [9-13]. ZnO has emerged to be more efficient catalyst as far as water detoxification is concerned because it generates H_2O_2 more efficiently, it has high reaction and mineralization rates [14, 15]. Also it has more numbers of active sites with high surface reactivity [16]. ZnO has been demonstrated as an improved photo catalyst as compared to commercialized TiO_2 based on the larger initial rates of activities and its absorption efficacy of solar radiations

[17]. However, ZnO has almost the same band gap (3.2 ev) as TiO_2. Surface area and surface defects play an important role in the photo catalytic activities of metal oxide. The reason is that, doping of metal oxide with metal and/or transition metals increases the surface defects [18]. In addition it affects the optical and electronic properties and can presumably shift the optical absorption towards the visible region [19]. This can subsequently activate these modified metal oxide photo catalysts upon visible light irradiation. Doping of ZnO with cobalt (Co) has been reported to cause hyper chromic shift in the optical absorption of ZnO, which is attributable to the shrinkage of the band gap [20]. These changes in ZnO caused by Co ion were assumed to play an important role in the photo catalysis. As reported ZnO is better solar photo catalyst than TiO_2 and other metal oxide on the basis of solar radiation absorption. In addition enhancement in the optical absorption owing to increase in surface defects by doping with Pb ion and Ag ion urge us to further investigate undoped and doped ZnO nano particles and its photo catalytic activities [18, 19]. Numerous studies report an improvement of visible-light photo catalytic activity of metal oxide semiconductors by doping with cations, anions, metals, and non-metals [21-25]. There are also some reports of the detrimental effect of dopants in the photo catalytic activity [26]. One of the strategies adopted for tuning the band gap is to employ suitable dopants by which the electronic structure of ZnO can be altered. The doping ions such as Al, Co, Ag, Pb and Mn have incorporated in ZnO and their effect has already been studied and reported [27-29]. The doping increase the bulk surface area and surface defects which generate more active sites for the reaction at an energy level lower than the conduction band of pure ZnO and thus absorbs visible light via these defect sites causing enhancement in the optical absorption of ZnO. ZnO is a good photo catalyst to degrade organic matter in water [30, 31, 32]. There are several methods for preparing nano sized ZnO powders such as spray pyrolysis, precipitation, thermal decomposition, hydrothermal synthesis and electrochemical growth [33-37]. Different methods yield different particle sizes of ZnO, depending on the type of precursor, the solvent, the pH and the temperature of the reacting solution. In this study, we employed a precipitation method to prepare metal doped Nano sized ZnO, which is the easiest method for producing nano material's and also carried out the photo catalytic experiments. The preliminary results presented in this work show much promise and suggest the need to further explore heterogeneous photo catalysis.

2. Experimental

2.1 Materials and methods

Acidal Navy Blue 3BR (ANB 3BR) C.I. 20470 from s d Fine-chem. Ltd. The starting materials, $Zn(CH_3COO)_2•2H_2O$ (s d Fine-chem. Ltd, >99.5%), Na_2CO_3 (Sisco Research Laboratories Pvt. Ltd, >99.9%), $Mn(CH_3COO)_2•4H_2O$ (Qualigens fine chemicals, >99%), $C_4H_6CuO_4.H_2O$ (s d Fine-chem. Ltd, >98%), $C_4H_6CoO_4.4H_2O$ (s d Fine-chem. Ltd, >99.5%), NaOH (Sisco Research Laboratories Pvt. Ltd, >98%) and HCl (Ranbaxy Fine Chemicals Ltd) were used as such. The chemical structure of the AB 10B are shown in Fig. 1.

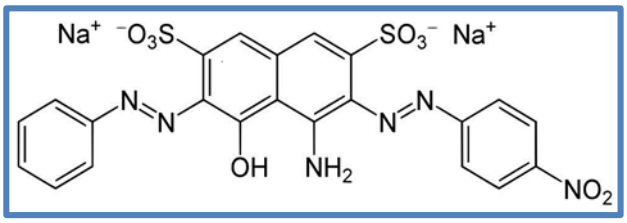

Figure 1. Chemical structure of ANB 3BR.

2.2 Catalyst preparation

Initially, the synthesis of zinc carbonate was attempted via the reaction $Zn(CH_3COO)_2*2H_2O + Na_2CO_3 \rightarrow ZnCO_3 + 2Na(CH_3COO)$. In a typical synthesis of undoped ZnO, 13.5 g of Zn $(CH_3COO)_2•2H_2O$ and 6.5g of Na_2CO_3 were separately dissolved in 50 ml of deionised water. Next, the Na_2CO_3 solution was added into the Zn $(CH_3COO)_2•2H_2O$ solution to form white precipitates. The precipitates were separated from the supernatant using a filtration and further washed with deionised water to remove reaction by-products until the salinity of the supernatant becomes less than 100 ppm. The separated precipitates were dried in air at 60°C and then heat treated at 300°C for 1 hour. For the synthesis of manganese, copper, cobalt-doped ZnO, a solid mixture of 0.25, 0.5, 0.75, 1 and 1.5 mol% Mn $(CH_3COO)_2•4H_2O$, $C_4H_6CuO_4.H_2O$, $C_4H_6CoO_4.4H_2O$ in $Zn(CH_3COO)_2•2H_2O$ was dissolved in 50 ml of deionised water and then mixed with an aqueous

solution of Na_2CO_3, followed by the same procedure as for undoped ZnO.

2.3 Analytical methods

IR spectra were recorded using Perkin Elmer 6X FT-IR spectrophotometer using KBr pellets. Diffuse reflectance spectra were recorded using Shimadzu UV-2450. Powder X-ray diffraction patterns of ZnO catalyst was obtained using X' per PRO diffractometer. Transmission electron microscope (TEM) images were recorded using a Philips model (Tecnai 10) transmission electron microscope. UV spectral measurements were done using Shimadzu UV 2101PC spectrometer. The pH values were measured via Digisun pH meter (Model 2001). The morphology of catalyst was examined using a HITACHI-SU6600 field emission scanning electron microscope (FE-SEM). Chemical oxygen demand (COD) was measured with a Merck COD- Spectroquant TR 320 model.

2.4 Irradiation procedure

All experiments were carried out under identical conditions using Heber visible annular type photo reactor model HVAR. The irradiation was carried out using Tungsten (500w) lamp. Dark reaction also carried out for the purpose of comparison. The catalyst was added to an aqueous dye solution and reaction mixture was continuously stirred by magnetic stirrer and for the complete mixing of the reaction solution. At specific time intervals, 4–5 mL of the sample was withdrawn and centrifuged to separate the catalyst. One millilitre of the sample was suitably diluted and its absorbance's at 619 nm and 322nm were measured immediately. Absorbance at 619 nm ($n \rightarrow \pi^*$) transition of –N= N– group is due to the color of the ANB 3BR solution and it is used to monitor the decolorisation of dye. The absorbance at 322 nm represents the aromatic content of ANB 3BR and the decrease of absorbance at 322 nm indicates the degradation of aromatic part of dye.

2.5 Adsorption isotherm of the dye molecules onto ZnO

The photo degradation of organics using semiconductor photo catalyst mainly occurs on the surface of catalyst [38]. It is important to study the adsorptive properties of doped and undoped ZnO using respective target compounds as adsorbate. The adsorption process of dissolved ANB 3BR dye onto doped and undoped ZnO nano particles was investigated in detail.

Adsorption equilibrium experiments were carried out with the required amount of catalyst dosage (0.05g/10 ml) and the concentrations of the ANB 3BR varied from 1 to 200 ppm. The systems were equilibrated for 24 h at 27 °C. There are quite a few common isotherms used for correlating adsorption equilibrium data [39]. Equilibrium adsorption data collected in this study could be fitted by both Langmuir and Freundlich isotherms. The common forms of these adsorption isotherm equations (1&2), respectively, are:

$$q_{eq} = \frac{K_L C_{eq}}{1+q_m C_{eq}} \quad (1)$$

$$q_{eq} = K_F C_{eq}^{\frac{1}{n}} \quad (2)$$

Where, q_{eq} (mg/g) and C_{eq} (mg/L) are the amount of adsorbed dye per unit weight of catalyst and unadsorbed dye concentration in solution at equilibrium, respectively. The constant K_L (L/g) is the Langmuir equilibrium constant and the K_L/q_m gives the theoretical monolayer saturation capacity, q_m. K_F (L/g) is the Freundlich constant and n (g/L) is the Freundlich exponent. The adsorption equilibrium data were analyzed by Langmuir and Freundlich isotherm model equations. The constants of Langmuir and Freundlich isotherms were also evaluated and tabulated in Table 1. The adsorption isotherm results from Figure 2 indicated that Langmuir isotherm fitted the data well ($r^2 > 0.95$).

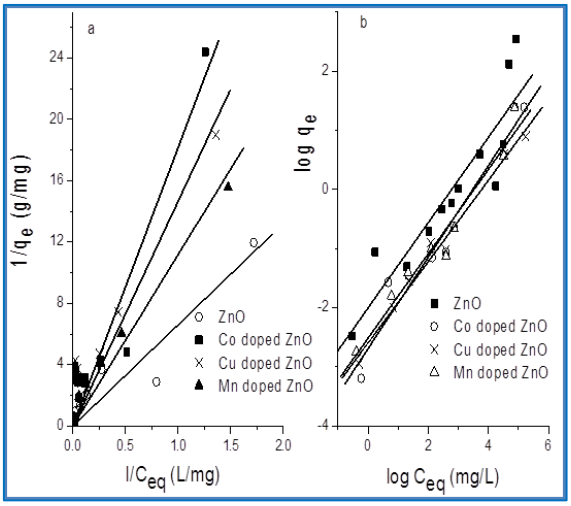

Figure 2. a) Langmuir and **b)** Fruendlich isotherm of

undoped and Mn, Cu, Co doped ZnO (catalyst dosage = 0.05 g/10 mL; pH = 7; T = 27°C; t=24h; agitation = 100 rpm).

The value of R_L, the separation factor fell in the range of 0–1 which clearly showed that the adsorption process is favourable. The value of n in Freundlich isotherm also varied from 1 to 10 which again proved that the adsorption is favourable.

nano particles. It seems that Co, Cu, Mn ions form complex with the ZnO surface oxygen, hence; suppress the growth of ZnO crystallite.

The diffuse reflectance spectra of ZnO and 0.25, 0.5, 0.75, 1, 1.5% of Cu, Co and Mn doped ZnO nano crystals catalysts are displayed in Fig. 6, respectively.

Table 1 The constants of Langmuir and Freundlich isotherms of ANB 3BR by visible light

Isotherms	ZnO	Mn - ZnO	Cu -ZnO	Co - ZnO
Langmuir				
q_m(mg/g)	1.7412	0.5640	0.5927	1.047
K_L	0.0939	0.1893	0.1322	0.056
R_L	0.9141 - 0.0505	0.8408 - 0.0257	0.8832 - 0.0364	0.947 - 0.082
r^2	0.9534	0.9607	0.9658	0.9547
Fruendlich				
K_F (L/g)	0.1353	0.083	0.0678	0.0809
N	1.3875	1.7319	1.2918	1.4009
r^2	0.9132	0.8349	0.9768	0.9791

3. Results and Discussions

3.1. Catalyst characterization

FE-SEM micrograph of the calcites (300 ºC) Mn, Cu, Co doped ZnO and undoped ZnO nano particles is shown in Fig. 3 (A, B, C and D). This image shows global and uniform particles which are coherent together. In Fig. 4 (A, B, C) shows the EDX data of Mn/TiO_2 three peaks around 0.5, 1 and 5.9 keV, Co/ZnO shows seven peaks around 0.5, 0.7, 1, 6.9, 7.7, 8.7 and 9.6 keV and Cu/ZnO shows six peaks around 0.5, 1, 8, 8.7, 8.9 and 9.6 keV respectively. The intense peak is assigned to the bulk ZnO and the less intense peaks to the surface ZnO. The peaks of Mn (0.5, and 5.9 keV), Co (0.7, 6.9 and 7.7 keV), Cu (1, 8 and 8.9 keV) are distinct in Fig. 4 (A, B, C). The less intense peak is assigned to Mn, Co, Cu in the ZnO lattices. These results confirmed the existence of Mn, Cu, and Co atoms in the solid catalysts but the XRD patterns do not show any peaks related to Mn, Cu, Co (even for 1.5% Mn, Cu, Co-doped ZnO catalyst). Therefore, it may be concluded that Mn, Cu and Co ions are uniformly dispersed among the ZnO crystallites.

Figure 5 (A and B, C, D) shows TEM image of samples from which the particle sizes of undoped and Co, Cu, Mn - doped ZnO and were found to be around 5-15 and 20-50 nm, respectively. Hence, it can be concluded that the addition of Co, Cu, Mn to Zinc hinders the growth of ZnO

ZnO nano crystals exhibited absorption in the UV range (200–400 nm). The band-gap energy E_{bg} of the photo catalyst is given by equation (3),

$$E_{bg} = \frac{1240}{\lambda} eV \quad (3)$$

Where, λ is the wavelength in nano meters. From the above equation the band-gab energy E_{bg} (2.95-3.35eV) of Cu doped ZnO, (2.78-3.44eV) of Co doped ZnO, (2.81-3.00eV) of Mn doped ZnO and 3.49 eV of undoped ZnO, respectively. ZnO nano crystal has slightly higher band gap than doped ZnO.

The XRD pattern of Co, Cu, Mn - doped ZnO and undoped ZnO nano crystals are given in Fig. 7, 8, 9 and 10. All the marked diffraction peaks of ZnO in Fig. 10 can coincidently be indexed by the known hexagonal standard ZnO. The crystallographic phase of these ZnO nano crystals belongs to the wurtzite-type ZnO. Characteristic peaks of ZnO at 32.24, 34.91, 36.73 and 57.06, correspond to (1 0 0), (0 0 2), (1 0 1) and (1 1 0) diffraction peaks of wurtzite ZnO, indicating that the ZnO shell possesses a hexagonal crystal structure. The relatively high intensity of the (1 0 1) peak is indicative of anisotropic growth and implies a preferred orientation of the crystallites. No significant difference could be observed between the XRD patterns of the doped and undoped ZnO. The average particle sizes of undoped and doped powders calcined at 300 °C for 1h

were calculated using Scherrer's equation (d=0.94 λ /β cos θ) as shown in table 2. Where, λ denotes the wavelength of the radiation equal to 0.154 nm, β the full width at half maximum (FWHM) and θ the half diffraction angle.

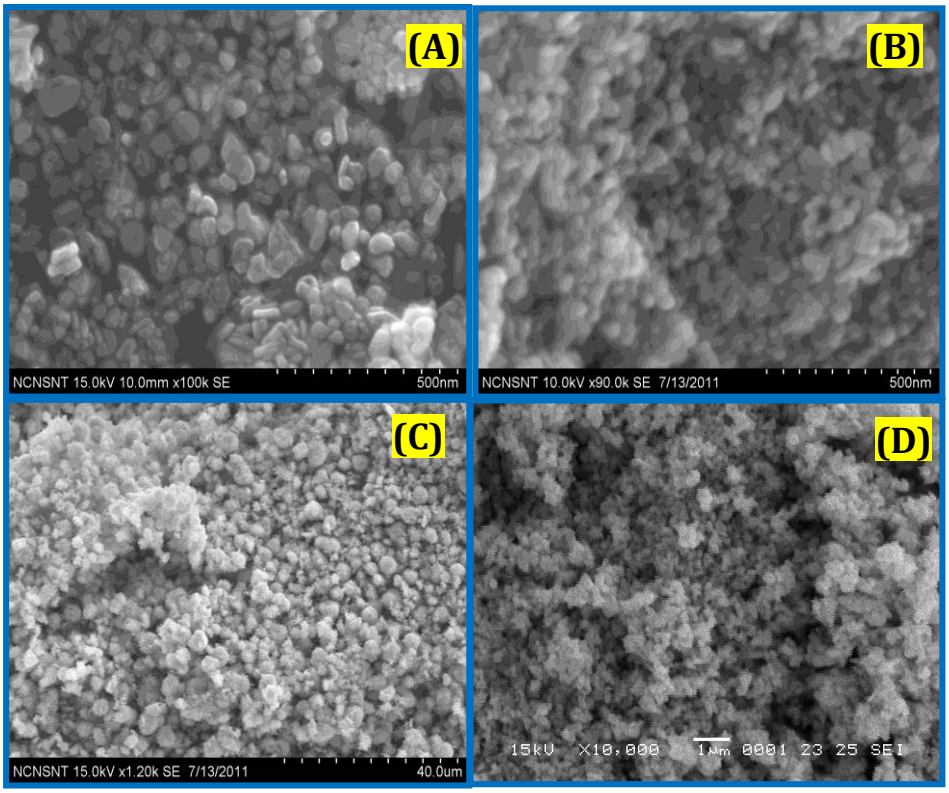

Figure 3. FE-SEM images of **A)** Mn doped ZnO **B)** Cu doped ZnO **C)** Co doped ZnO and **D)** ZnO calcite at 300°C for 1h.

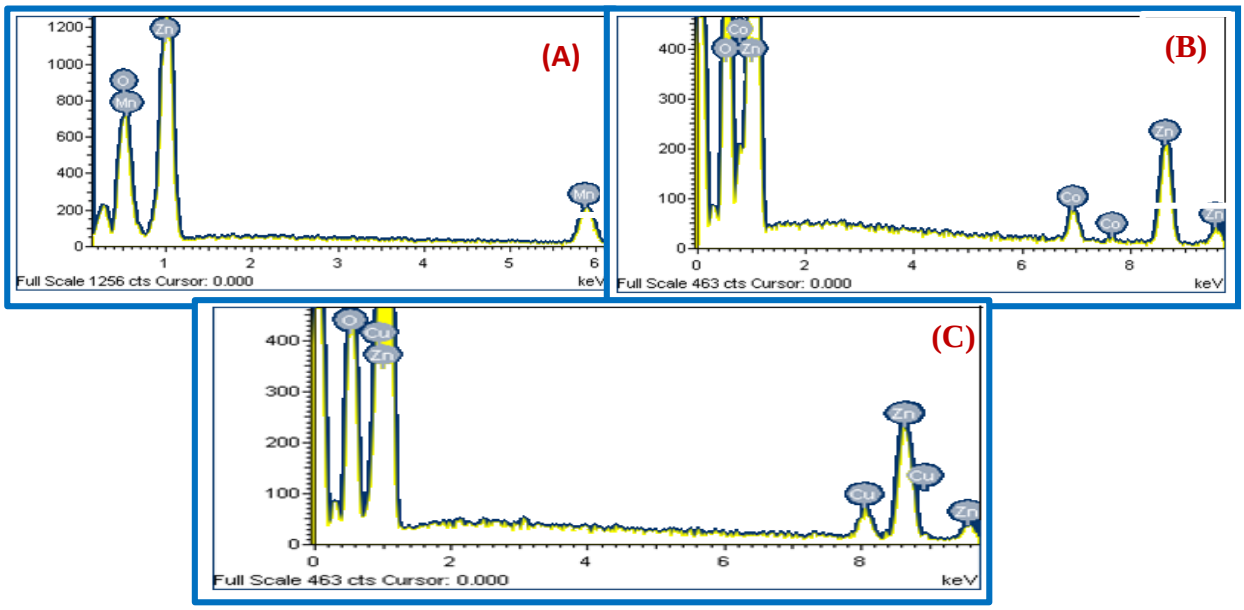

Figure 4. EDX images of **A)** Mn doped ZnO **B)** Co doped ZnO and **C)** Cu doped ZnO.

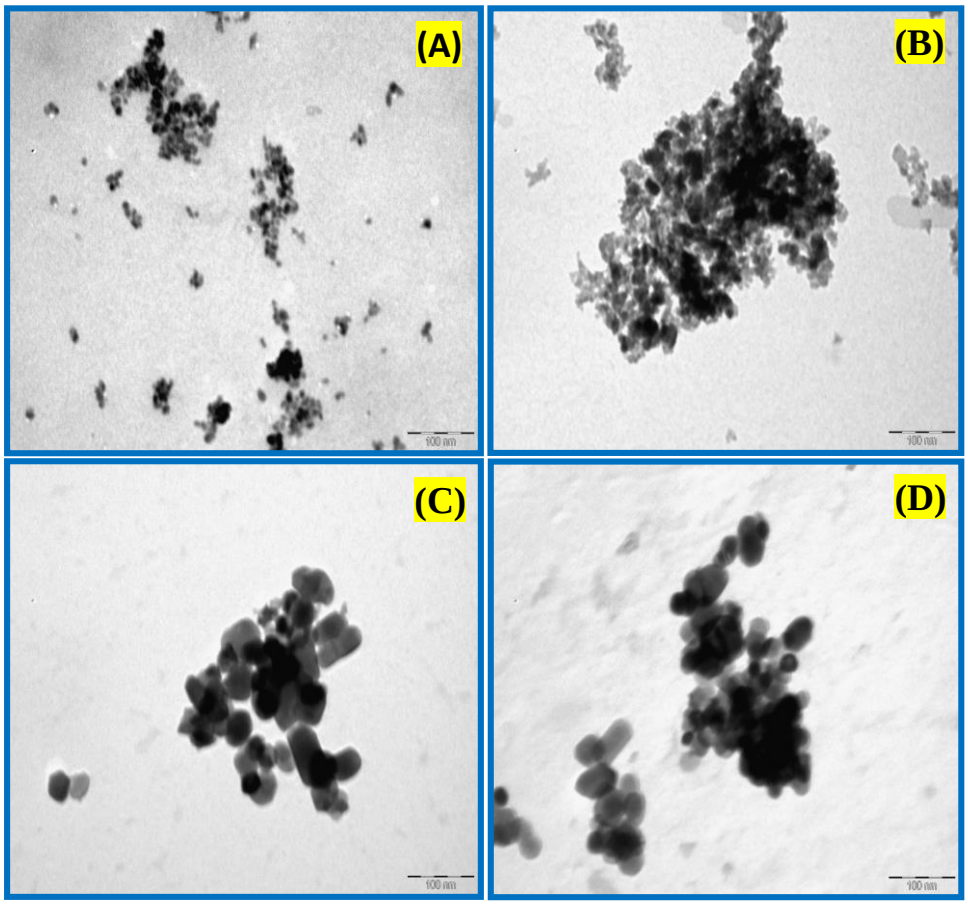

Figure 5. TEM images of **A)** ZnO **B)** Co doped ZnO **C)** Cu doped ZnO and **D)** Mn doped ZnO calcite at 300°C for 1h.

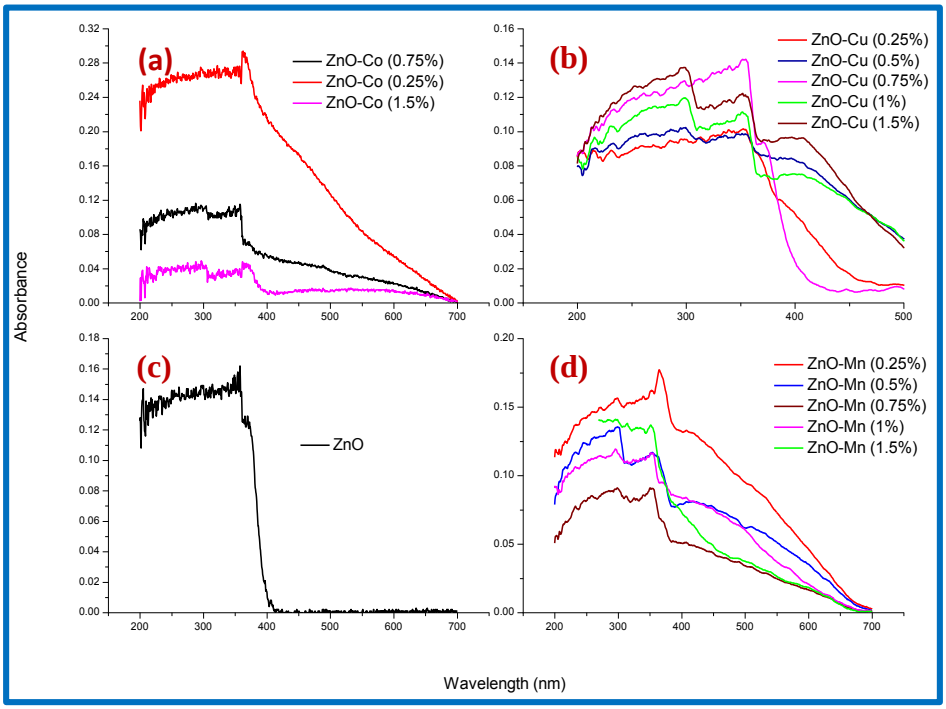

Figure 6. The diffuse reflectance spectra (DRS) of undoped and Mn, Cu, Co doped ZnO

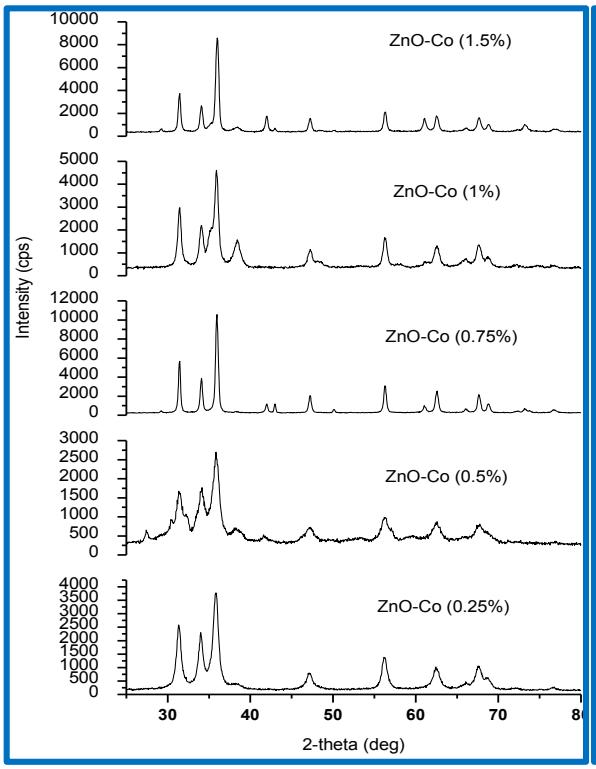

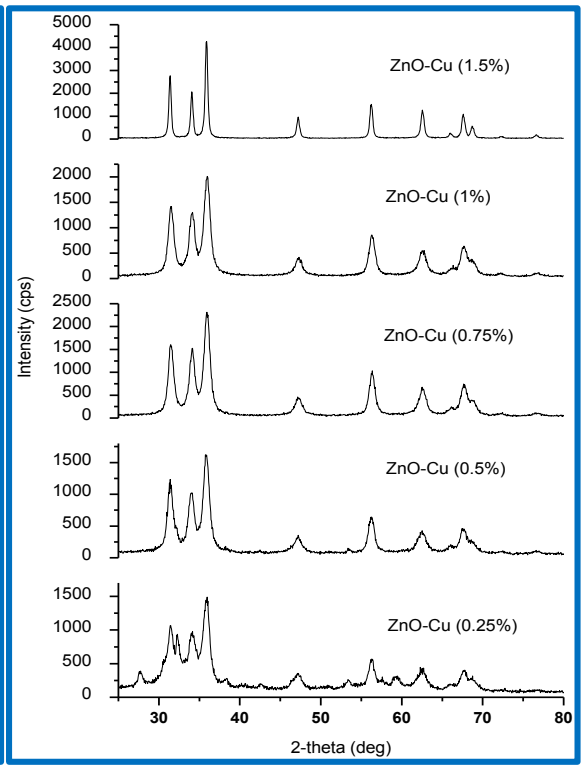

Figure 7. X-ray diffraction pattern of Co doped ZnO. Figure 8. X-ray diffraction pattern of Cu doped ZnO.

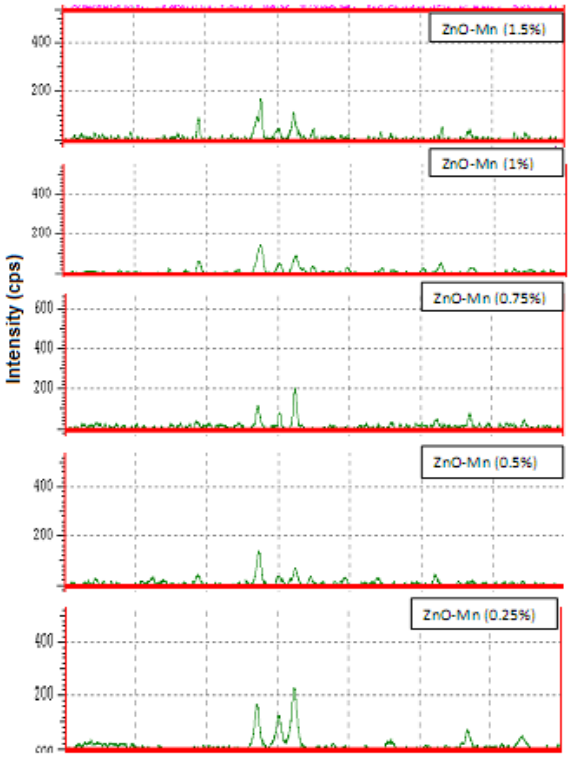

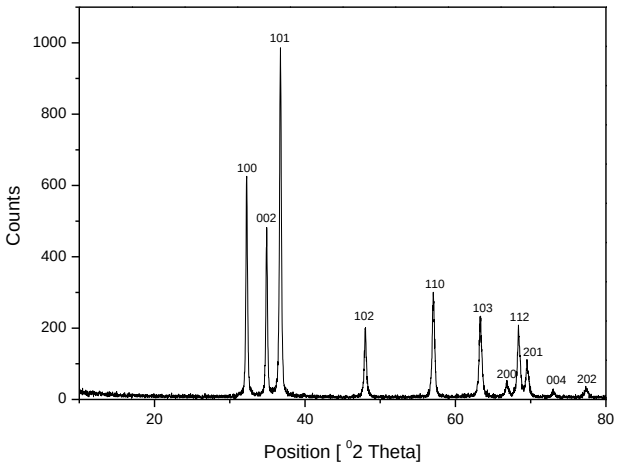

Figure 9. X-ray diffraction pattern of Mn doped ZnO Figure 10. X-ray diffraction pattern of ZnO.

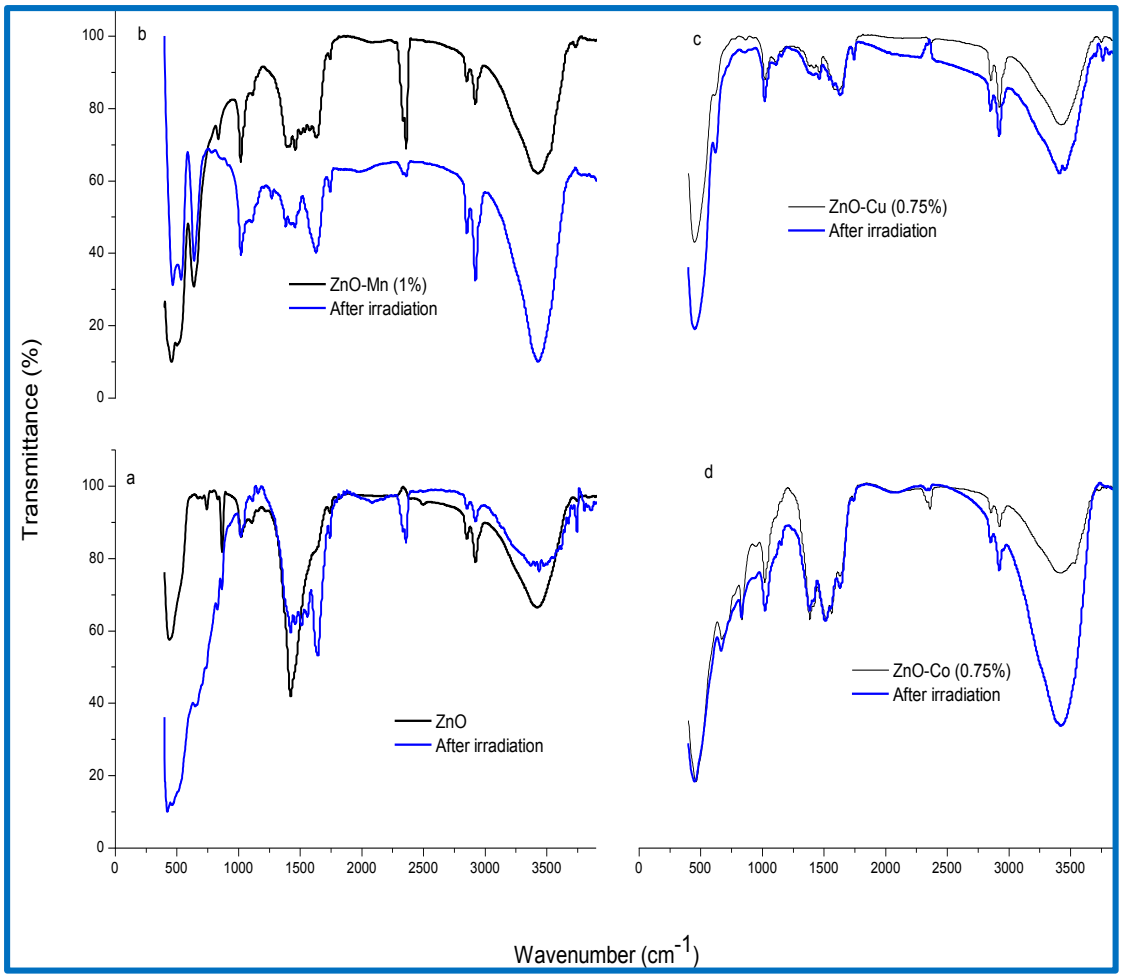

Figure 11. FT-IR spectra of **A)** ZnO **B)** Mn doped ZnO **C)** Cu doped ZnO and **D)** Co doped ZnO and after visible irradiation.

Table 2 Particle sizes for undoped and Mn, Cu, Co doped ZnO

Catalyst	Doping level (mole %)	Particle sizes (nm)
ZnO	0	8-10
Mn-ZnO	0.25	8-13
	0.5	8-9
	0.75	8-15
	1	8-218
	1.5	8-217
Cu-ZnO	0.25	5-29
	0.5	5-14
	0.75	15-110
	1	6-11
	1.5	32-72
Co-ZnO	0.25	2-14
	0.5	2-15
	0.75	6-55
	1	6-15
	1.5	6-55

Fig. 11(a, b, c, d) give the FT-IR spectra of undoped and doped ZnO nano crystals. Figure 11a indicated the presence of absorption bands at 438 cm^{-1} confirming the presence of Zn-O (metal-oxide) bond. Fig. 11(a, b, c, d) shows the absorption band at 2350 cm^{-1} confirming the absorption of atmospheric CO_2 on the metallic cations [40, 41]. As reported earlier the band in the region of 680–400 cm^{-1} is characteristic of ZnO nano crystals [42]. Figure 11b shows the presence of absorption bands at 1629 cm^{-1} confirming the oxide from Zn-O bond. The peak at 1454 - 1400cm^{-1} indicates symmetric stretching vibration of coo. 454 cm^{-1} and 644 cm^{-1} indicates bending and stretching vibration of Mn-O. Absorption bands observed at 2925 cm^{-1} and 3400cm^{-1} represent C-H and O-H respectively. Fig. 11 (a, b, c, d) indicates the absorption peaks at 1400-1600cm^{-1} correspond to C=O stretching mode.

3.2. Catalytic activity

pH is an important parameter in photo catalytic degradation. The effect of pH on the photo degradation of ANB 3BR was studied in the pH range of 1.5–11.5. After 6h of irradiation 99.8, 99.8, 98.2 and 97.6% of degradation for ZnO, Mn, Cu, Co doped ZnO nano crystals at neutral pH (Fig. 12). The maximum efficiency was observed at neutral pH of 7. In acidic pH range (1.5–3.5) the removal efficiency is less and it may be due to the dissolution of ZnO [43]. ZnO nano crystals can react with acids to produce the corresponding salt at acidic pH. The adsorption of dye at different pH in dark was measured. The percentages of adsorption at pH 7 were 20.4, 24.9, 20.69 and 17.5 for ZnO, Mn, Cu, Co doped ZnO, respectively. Adsorption of dye molecule is maximum at pH 7 and it decreases at pH 9.5 and 11.5. Hence the degradation is also efficient at pH 7. It is highly advantageous to have the maximum efficiency at neutral pH 7 since there is no need of pre-treatment of the effluent.

Fig 13 the influence of the photo catalyst dosage on the degradation of ANB 3BR has been investigated employing different amounts of ZnO, Mn, Cu, Co doped ZnO nano crystals. The increase of catalyst dosage from 1 to 5 g L^{-1} increases the percentage degradation appreciably. Further increase of catalyst dosage above 5 g L^{-1}, decreases the percentage degradation. Hence 5 g L^{-1} of ZnO, Mn, Cu, Co doped ZnO catalyst concentration was used in the reusability experiments. The decrease at higher concentration may be due to aggregation of catalyst and its screening effect [44, 45].

The effect of pollutant concentration is a very important parameter in wastewater treatment. The effect of initial ANB 3BR concentration was investigated over the concentration range of 5 to 100 ppm. The experimental results are presented in Fig. 14. The results show that the increase in the dye concentration decreases the degradation and from the Fig. 14, it is clear that the degradation decreases with increase in the initial concentration of ANB 3BR. Similar results have been reported for the photo catalytic oxidation of other dyes [46–48]. The initial concentration dependence on the photo degradation of ANB 3BR may be due to the following reasons. When the dye concentration increases the amount of dye adsorbed on the catalytic surface increases. This affects the catalytic activity of the photo catalyst. The increase in dye concentration also decreases the path length of photon entering into the dye solution. At high dye concentration the dye molecules may absorb a significant amount of visible light rather than the catalyst and this may also reduce the catalytic efficiency [49].

3.3. Kinetics of visible Photo catalytic Decolourisation of AB 10B

The kinetics of photo decolourisation of various concentrations of ANB 3BR in visible irradiation is demonstrated in figures (15-18). From the figure it could be inferred that the photo degradation experiments of ANB 3BR by visible light employing ZnO, Mn, Cu, Co doped ZnO nano crystals as the photo catalyst exhibited pseudo-first-order kinetics with respect to the concentration of the dye. The kinetics of photo decolourization of ANB 3BR could be represented by the following equations.

$$-d[\text{ANB 3BR}]dt = k_{obs}[\text{ANB 3BR}] \quad (4)$$

$[\text{ANB 3BR}] = [\text{ANB 3BR}]_0$ at t=0 could be deduced from Equation (4) upon integration and hence

$$\ln[\text{ANB 3BR}]_0/[\text{ANB 3BR}] = k_{obs}t \quad (5)$$

Wherein, k_{obs} are the pseudo-first-order rate constant. Figure 19 is the plot of $\ln([\text{ANB 3BR}]_0/[\text{ANB 3BR}])$ or $\ln(C_0/C)$ Vs irradiation time for different initial concentrations of ANB 3BR. The values of k_{obs} calculated employing least square regression analysis and half life t½ (minutes) i.e., t½ = 0.693/k for all the above experiments is given Table 3. The rate of photo degradation followed pseudo-first-order kinetics in which the value of the kinetic constant decreased with increase in the concentration of the initial reactant. This could be due to the decrease in the number of active sites on the catalyst surface due to the adsorption of the dye molecules. The rate constant (k_{obs}) was calculated from the slopes of the plots (see Table 3) to study the nature of the photochemical reaction of ANB 3BR with ZnO and Mn, Cu, Co doped ZnO nano crystals.

3.4. UV-VIS absorption spectrum

Figure 20 shows the UV-VIS absorption spectrum of undoped and doped ZnO recorded for 10 ppm ANB 3BR solution visible irradiated for different durations. The maximum absorbance values recorded during the photo decolourization and degradation process showed a decrease with increase in irradiation time.

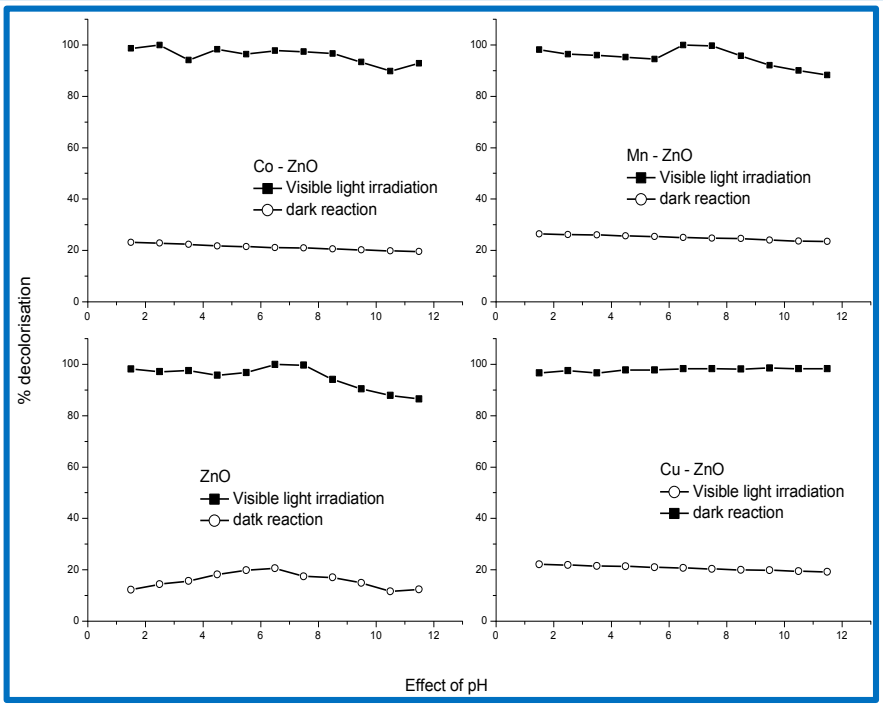

Figure 12. Effect of pH on the dark and visible photo catalytic decolorisation of ANB 3BR using undoped and doped ZnO as the photo catalyst. [Dye] = 10 ppm; Mass of catalyst = 5 g/L; Duration of visible irradiation = 6 hrs.

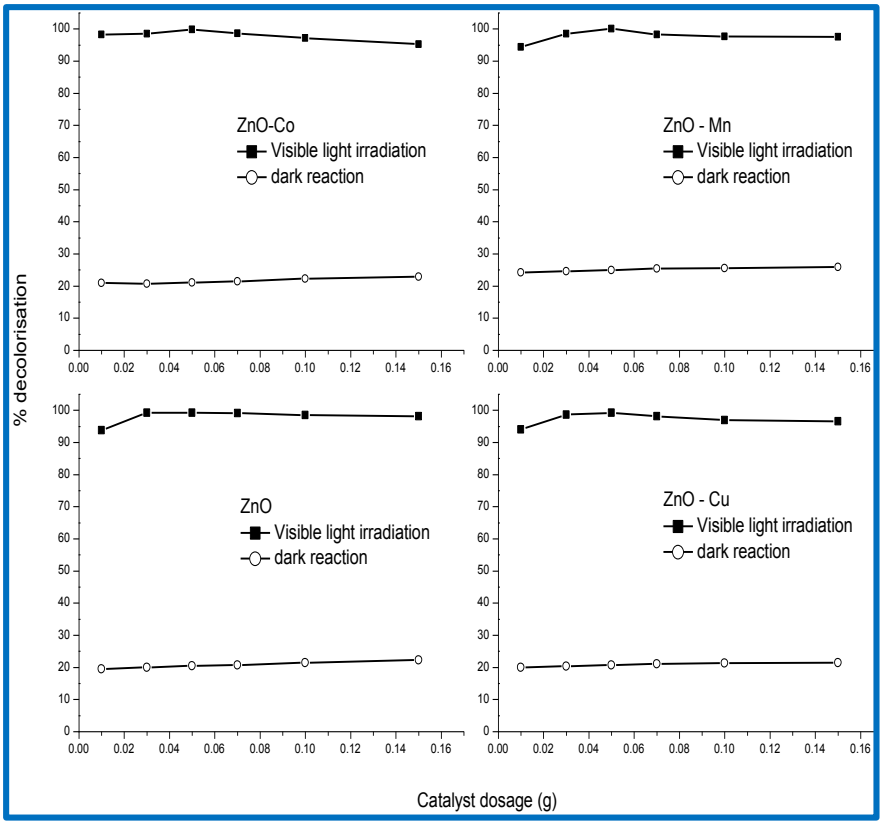

Figure 13. Effect of catalyst loading on the dark and visible photo catalytic decolourization of ANB 3BR using undoped and doped ZnO as the photo catalyst. [Dye]= 10 ppm; pH=7; Duration of solar irradiation = 6 hrs.

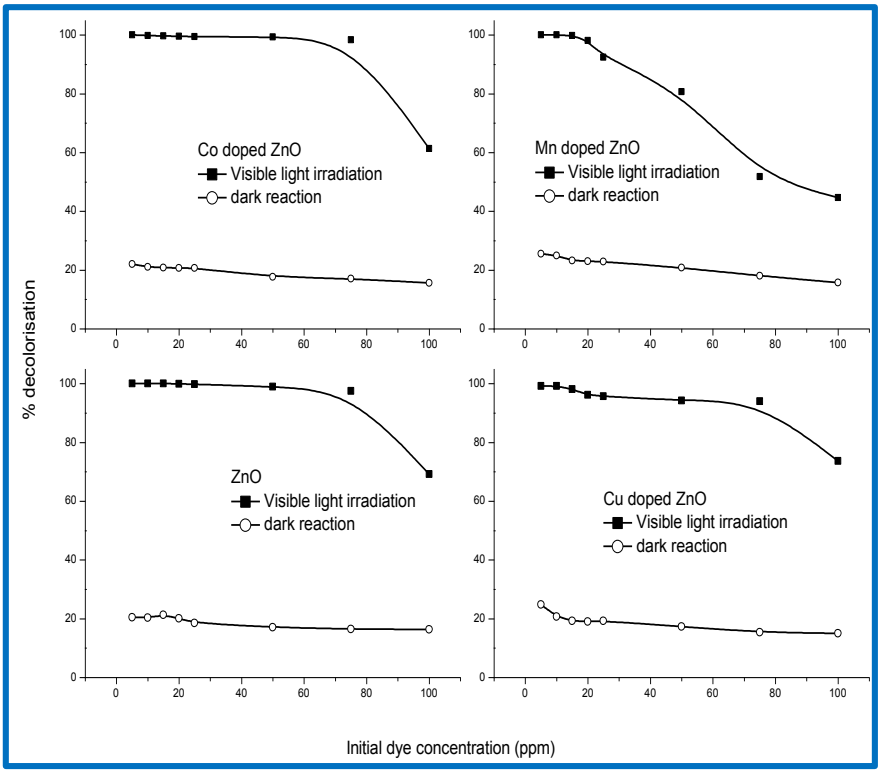

Figure 14. Effect of initial dye concentration in the dark and visible photo catalytic decolorisation of ANB 3BR using undoped and doped ZnO as the photo catalyst. pH=7; Mass of catalyst= 5 g/L; Duration of visible irradiation = 6 hrs.

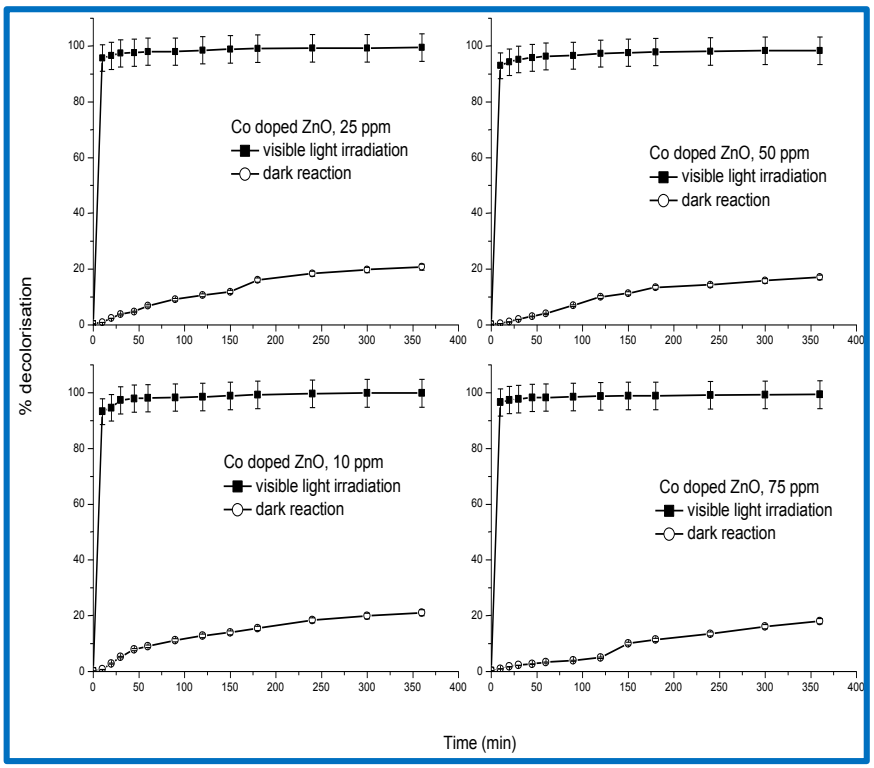

Figure 15. Kinetics of dark and visible photo decolourisation of dye using Co doped ZnO as the photo catalyst. [Dye]= 10 ppm, 25 ppm, 50 ppm, 75 ppm; pH=7; Mass of catalyst = 5 g/L.

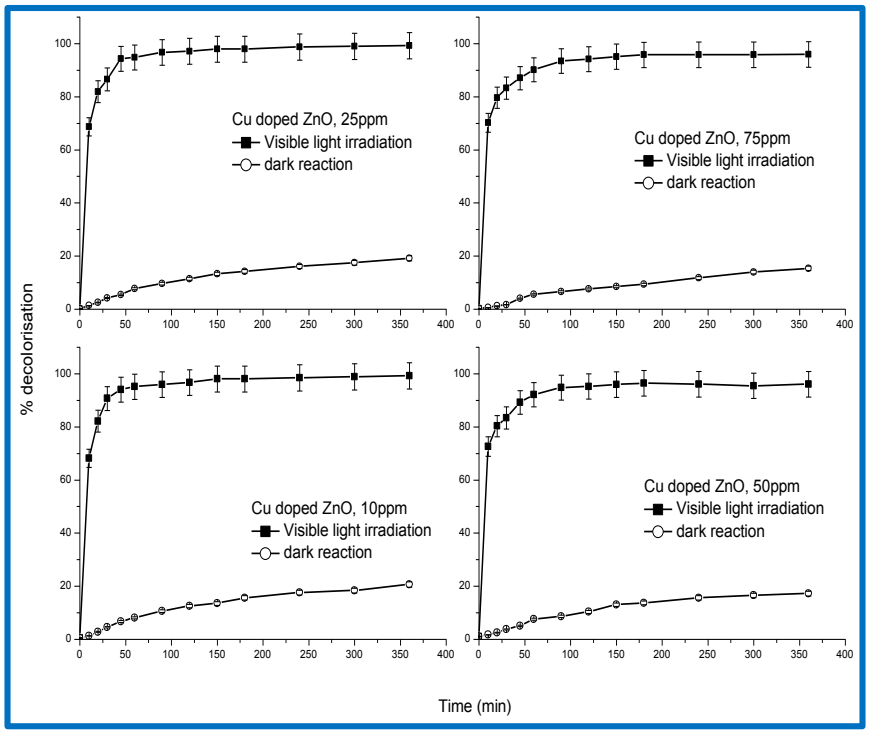

Figure 16. Kinetics of dark and visible photo decolourisation of dye using Cu doped ZnO as the photo catalyst. [Dye]= 10 ppm, 25 ppm, 50 ppm, 75 ppm; pH=7; Mass of catalyst = 5 g/L.

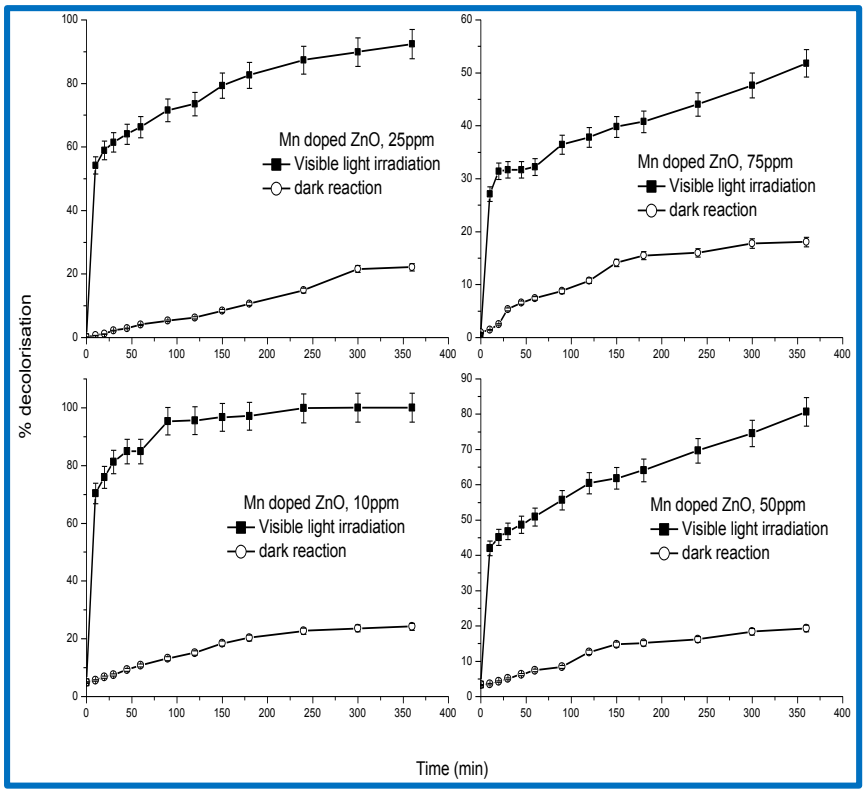

Figure 17. Kinetics of dark and visible photo decolourisation of dye using Mn doped ZnO as the photo catalyst. [Dye]= 10 ppm, 25 ppm, 50 ppm,75 ppm; pH=7; Mass of catalyst = 5 g/L.

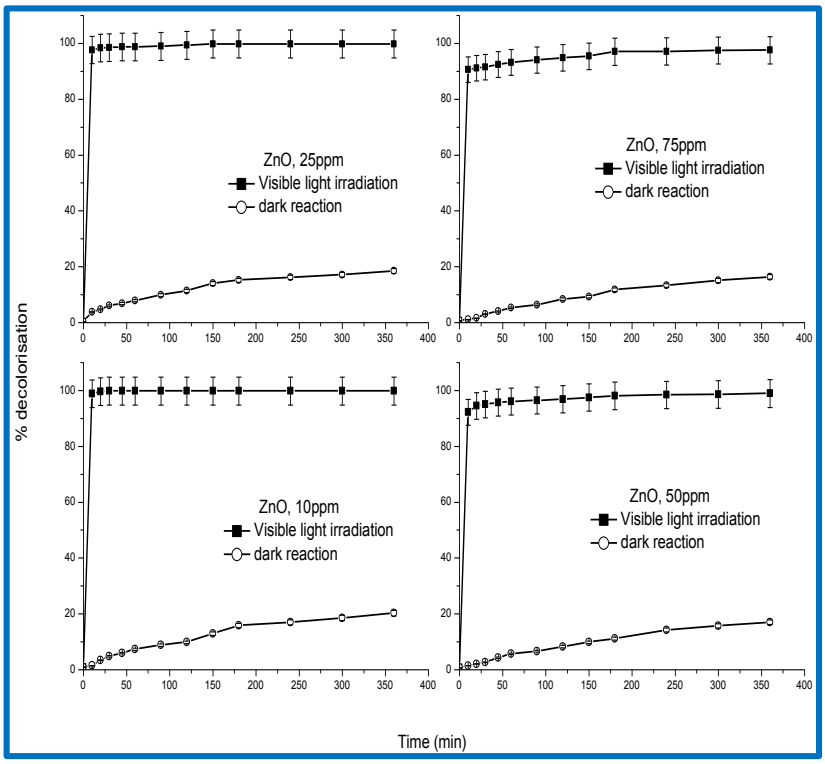

Figure 18. Kinetics of dark and visible photo decolourisation of dye using ZnO as the photo catalyst. [Dye]= 10 ppm, 25 ppm, 50 ppm,75 ppm; pH=6.8; Mass of catalyst = 5 g/L.

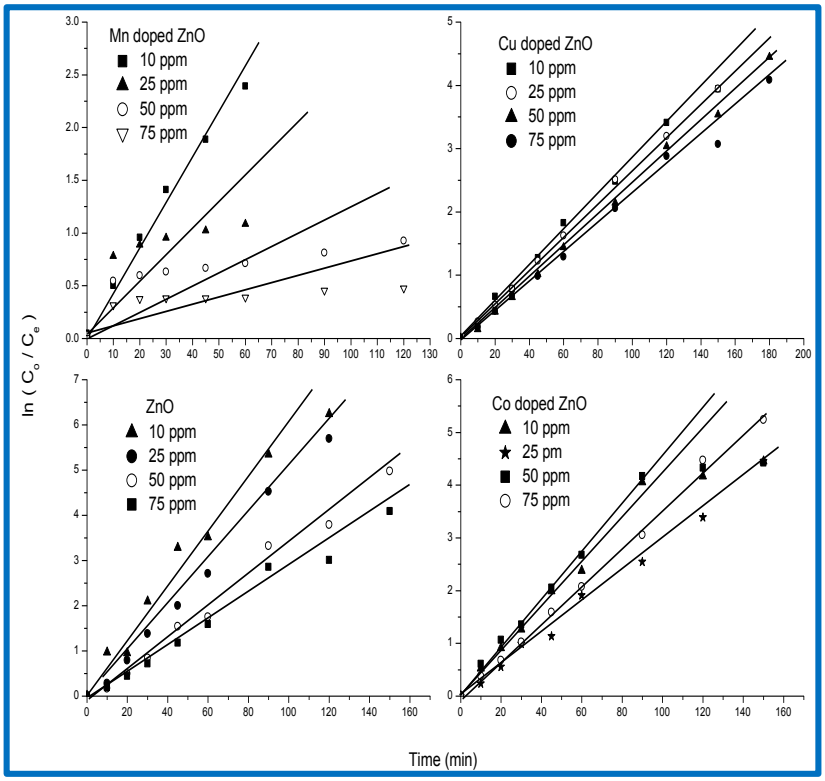

Figure 19. Pseudo first order kinetic plot of visible photo decolorisation of ANB 3BR by undoped and Mn, Cu, Co doped ZnO for different initial dye concentrations. Mass of catalyst = 5g/L.

Table 3 Pseudo first order rate constants & half life of ANB 3BR decolourisation by Visible light

Dye concentration, [ppm]	Rate constants, k (min^{-1})				Half life, $t_{1/2}$ (min^{-1})			
	ZnO	Mn-ZnO	Cu-ZnO	Co-ZnO	ZnO	Mn-ZnO	Cu-ZnO	Co-ZnO
10	0.2449	0.0411	0.0605	0.0639	2.8	16.86	11.45	10.84
25	0.1000	0.0235	0.0474	0.0410	6.93	29.48	14.62	16.90
50	0.0723	0.0099	0.0408	0.0292	9.58	70	16.98	23.73
75	0.0609	0.0054	0.0383	0.0207	11.37	128.33	18.09	33.47

The absorption peak of the spectra rapidly decreased with increase in duration of visible irradiation and almost disappeared as shown in figure 20. The chromophores responsible for characteristic colour of the ANB 3BR were broken down resulting in the degradation of ANB 3BR and also the absorption peak decreases at 322nm it conforms the aromatic part will be degraded. Results indicated that synthesized ZnO and Mn, Cu, Co doped ZnO nano crystals showed high photo catalytic activity since 100% degradation was observed for lower concentrations of ANB 3BR.

3.5. Effect of Na_2CO_3 and NaCl

The other chemicals used in the dye industry play a vital role in the dyeing process. Na_2CO_3 is added to adjust the pH of the dye bath which is important in fixing the dye on the fabrics and in the fastness of colour. Sodium chloride is mainly used in the dyeing process for the transfer of dye stuff to fabric [50]. Therefore, the dye industry wastewater contains a considerable amount of carbonate and chloride ions. Hence, it is important to study the influence of CO_3^{2-} and Cl^- ions in the photo catalytic degradation.

The effect of addition of Na_2CO_3 on the photo catalytic oxidation of ANB 3BR is shown in Fig. 21. Increase in the Na_2CO_3 addition decreases the degradation efficiency. Addition of 0.5, 1, 1.5 and 2 wt% Na_2CO_3 decreases the decolourisation at 4h. Similar observations have been reported earlier in the literature [51, 52]. The decrease in degradation efficiency of the dye is due to hydroxyl radical scavenging property of carbonate ion as shown in the following equations (6&7),

$$CO_3^{2-} + .OH \rightarrow OH^- + CO_3^{\cdot-} , \quad (6)$$

$$HCO_3^- + .OH \rightarrow H_2O + CO_3^{\cdot-} . \quad (7)$$

Thus the primary oxidant hydroxyl radical decreases gradually with the increase in carbonate ion and consequently there is a significant decrease in photo catalytic degradation.

The influence of Cl^- on the photo catalytic oxidation of ANB 3BR has been studied using NaCl. The results are shown in Fig. 21. Increase of the addition of Cl^- ion up to 2 wt% to the reaction solution decreases the decolourisation at 4h. A similar observation was reported in the organic pollutant degradation [53]. The decrease in decolourisation efficiency in the presence of chloride ion is due to the hole scavenging properties of chloride ion.

$$Cl^- + h^+_{VB} \rightarrow Cl^{\cdot} , \quad (8)$$

$$Cl^- + Cl^- \rightarrow Cl_2^{\cdot-} . \quad (9)$$

The reaction of dye molecule with the hole has to compete with this reaction (Eq. (8)). The chloride radical anions formed can also block the reactive sites of the catalyst surface. The inhibitory effect of chloride and phosphate ion on the photo catalytic degradation has been reported [54]. The inhibiting effect of CO_3^{2-} ion is greater than the inhibiting effect of Cl^- ion.

3.6. COD analysis

To find out the complete degradation of AB 10B, COD was determined for the experimental solutions after irradiation. Fig. 22 indicates the % COD removal increased after 360 min irradiation with ZnO and Mn, Cu, Co doped ZnO nano crystals. This confirms the mineralization of dye.

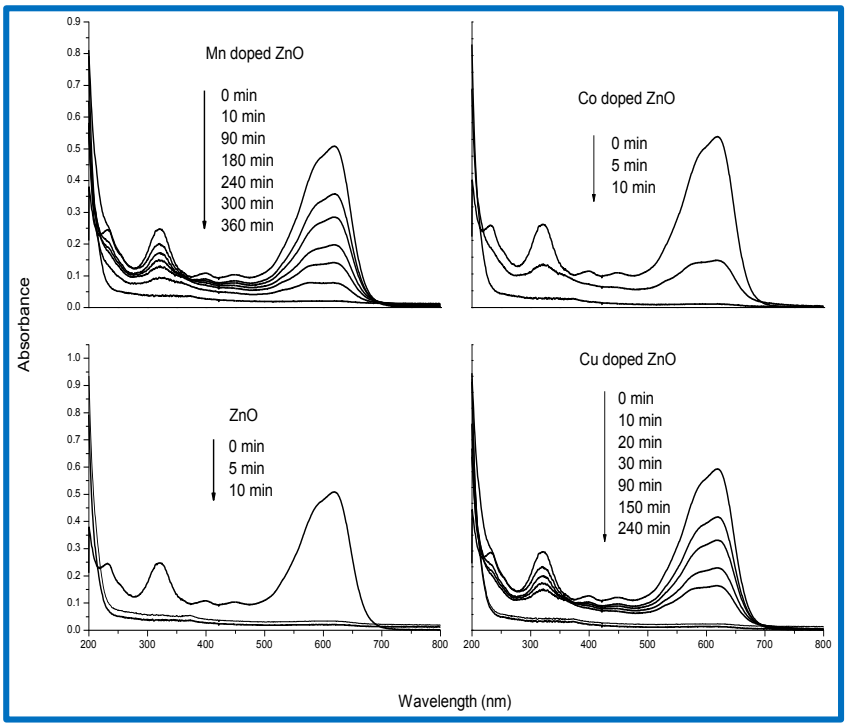

Figure 20. UV-VIS absorption spectrum of ANB 3BR during visible photo catalytic decolorisation in the presence of undoped and doped ZnO. $[AB]_0$ =10 ppm; Mass of catalyst = 5 g/L; pH= 7.

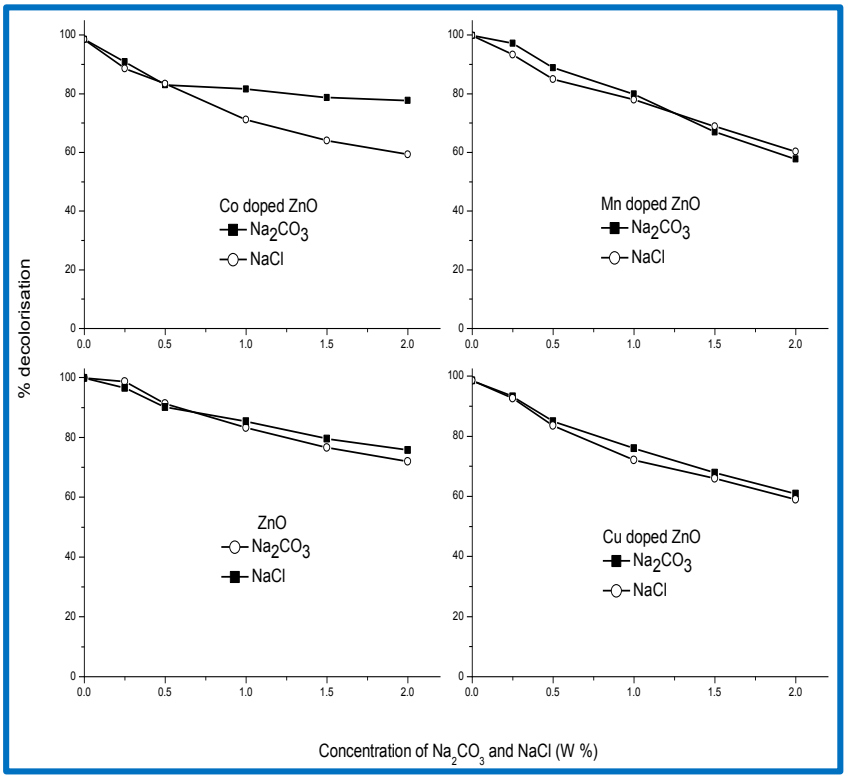

Figure 21. Effect of Na_2CO_3 & NaCl on Photo decolorisation of ANB 3BR dye by undoped and doped ZnO. [Dye]= 10 ppm; pH=7; Mass of catalyst =5 g/L.

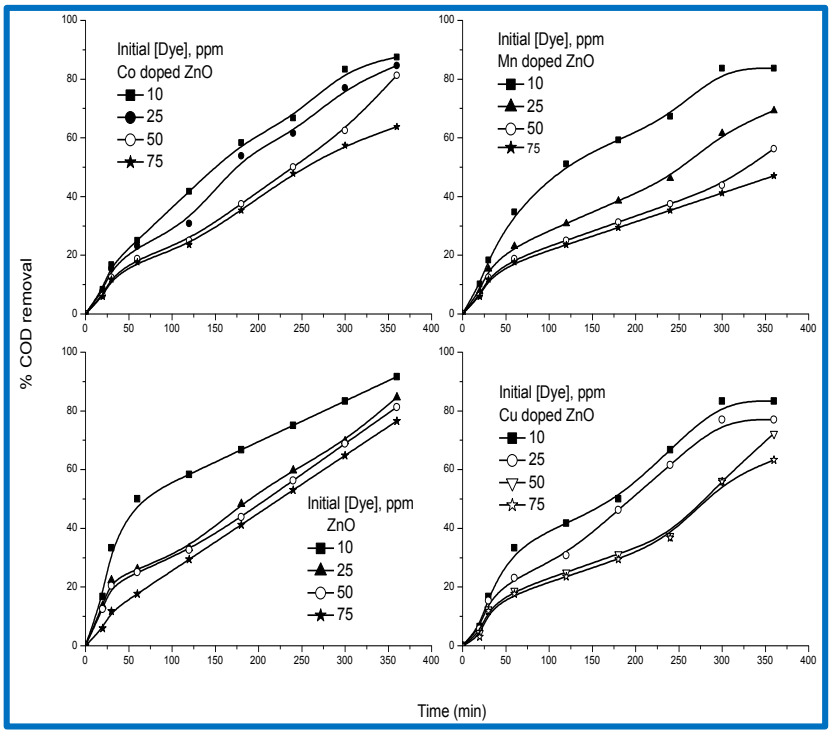

Figure 22. Reduction in % COD removal of the dye solution at various concentrations.

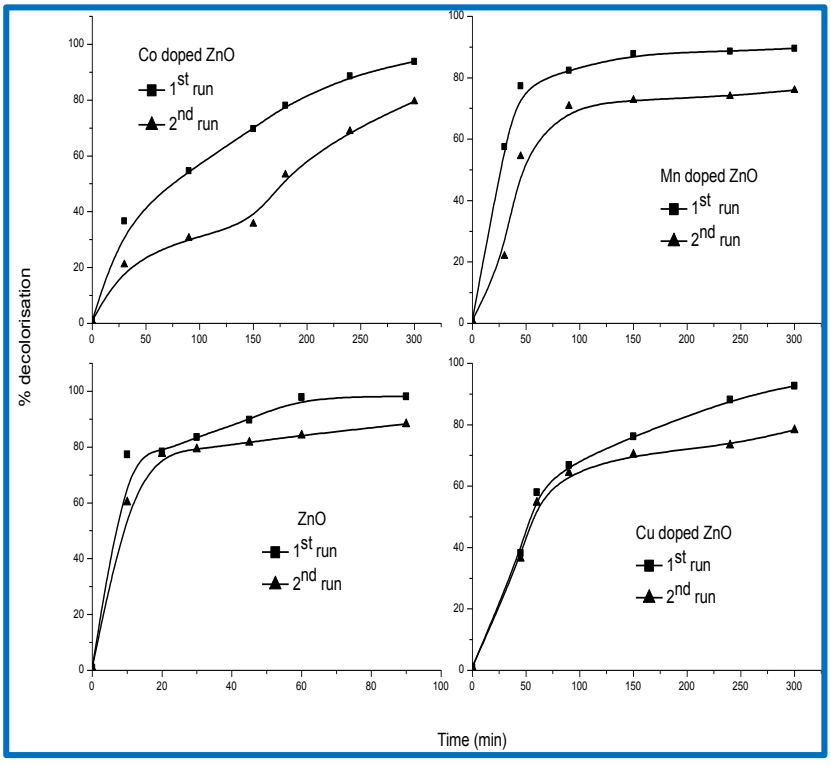

Figure 23. Reusability of the catalyst on the decolorisation of ANB 3BR for two runs by undoped and doped ZnO. [Dye]= 10 ppm, pH=7, Mass of catalyst =5 g/L, irradiation time = 300 min.

3.7. Reusability property

Reusability study is an important parameter for the degradation of toxic pollutants [55-56]. The stability of ZnO and Mn, Cu, Co doped ZnO nano crystals has been

studied. Degradation study was carried out for two runs with the catalyst recovered after each run. The entire catalytic stability test has been carried out under identical reaction conditions. After complete degradation, the catalyst was separated and washed with large amount of deionised water. The washed catalyst was dried in atmospheric conditions and in hot air oven at 100^0C for 30 min and used for second run. Fig. 23 show ANB 3BR degradation results of ZnO and Mn, Cu, Co doped ZnO nano crystals respectively for two runs. ZnO nano crystals exhibit remarkable photo stability as the degradation percentage is around 88% even in second cycle for 90 min. But Mn, Cu and Co doped ZnO nano crystals shows 75%, 78% and 79% of degradation in this second runs for 300 min. Furthermore ZnO and Mn, Cu, Co doped ZnO nano crystals are quite easily separated in a short time. This shows that ZnO and Mn, Cu, Co doped ZnO nano crystals can be easy recovered and reused.

4 Conclusions

Mn, Cu, Co doped ZnO and undoped ZnO nano crystals prepared by precipitation method and calcined at 300^0C effectively catalyze the degradation of ANB 3BR under visible light. The undoped and doped oxide has been characterized by XRD, EDX, FE- SEM, TEM, FT-IR, UV–visible DRS. Doping shifts the optical absorption edge to the visible region and reduces the intragranular resistance as well as the recombination of photo generated electron–hole pairs. In doped ZnO the degradation efficiency decreases compare to undoped ZnO because of the particle sizes increases and band gap decreases by adding metal ions. The photo catalytic decolourization of ANB 3BR was favourable in neutral pH. The absence of dye molecules on the catalyst surface after visible irradiation was confirmed by FT-IR supporting the reusability of the catalyst. Adsorption isotherm data well fitted with the Langmuir adsorption equilibrium models. The value of separation factor R_L of Langmuir isotherm was well in between 0 and 1 confirming the absorption process as favourable. The Freundlich constant (n) fell between 1 and 10 indicating that the adsorption process was favourable. The solar photo decolourization of ANB 3BR was found to exhibit pseudo first order kinetics.

.

References

[1] R. Asahi, T. Morikawa, T. Ohwaki, K. Aoki, Y. Taga, Visible-light photocatalysis in nitrogen-doped titanium oxides, *Science,* 293 (2001) 269-71.

[2] M.R. Hoffman, S.T. Martin, W. Choi, D.W. Bahnemann, Environmental Applications of Semiconductor Photocatalysis, *Chemical Reviews*, 95 (1995) 69-96.

[3] A. Mills, S.L. Hunte, An overview of semi-conductor photocatalysis, *Journal of Photochemistry and Photobiology A: Chemistry***,** 108 (1997) 1-36.

[4] C. Hu, Y. Tang, J. Yu, P. Wong, Photocatalytic degradation of cationic blue. X-GRL adsorption on TiO_2/SiO_2 photocatalyst, ***Applied*** *Catalysis* ***B****: Environmental*, 40 (2003) 131-140.

[5] H. Yamashita, M. Harada, J. Misaka, M. Takeuchi, K. Ikeue, M. Anpo, Degradation of propanol diluted in water under visible light irradiation using metal ion-implanted titanium dioxide photocatalysts, *Journal of Photochemistry and Photobiology A: Chemistry,* 148 (2002) 257-261.

[6] T. Tsuzuki, J.S. Robinson, P.G. Mc Cormick, UV-Shielding Ceramic Nanoparticles Synthesised by Mechano chemical Processing, *Journal of the Australian Ceramic Society*, 38 (2002) 15-19.

[7] A.C. Dodd, A.J. McKinley, T. Tsuzuki, M. Saunders, Tailoring the Photocatalytic Activity of Nanoparticulate Zinc Oxide byTransition Metal Oxide Doping, *Materials Chemistry and Physics*, 114 (2009) 382-386.

[8] J. Han, P. Mantas, A. Senos, Defect chemistry and electrical characteristics of undoped and Mn-doped ZnO, *Journal of the European Ceramic Society*, 22 (2002) 49-59.

[9] M. Afzaal, M.A. Malik, P. O'Brien, Preparation of zinc containing materials, *New Journal of Chemistry*, 31 **(**2007**)** 2029-2040.

[10] P.V. Kamat, Nanostructure Architectures for Solar Energy Conversion, *Journal of Physical Chemistry C*, 111 (2007) 2834–2860.

[11] A. Mills, J. Wang, Simultaneous Monitoring of the Destruction of Stearic Acid and Generation of Carbon Dioxide By Self-cleaning Semiconductor Photocatalytic Films, *Journal of Photochemistry and Photobiology A: Chemistry*, 182 (2006) 181-186.

[12] L. Vayssieres, Growth of Arrayed Nanorods and Nanowires of ZnO from Aqueous Solutions, *Advanced Materials*, 15 (2003) 464-466.

[13] P. Periyat, S.C. Pillai, D.E. McCormack, J. Colreavy, S.J. Hinder, Improved High-Temperature Stability and Sun-Light-Driven Photocatalytic Activity of Sulfur-Doped Anatase TiO_2, *Journal of Physical Chemistry C*, 112 (2008) 7644-7652.

[14] E.R. Carraway, A.J. Hoffman, M. Hoffmann, Photocatalytic Oxidation of Organic Acids on Quantum-Sized Semiconductor Colloids, *Environmental Science & Technology*, 28 (1994) 786–793.

[15] I. Poulios, D. Makri, X. Prohaska, Photocatalytic treatment of olive milling waste water oxidation of protocatechuic acid, *Global NEST Journal,* 1 (1999) 55–62.

[16] B. Pall, M. Sharon, Enhanced photocatalytic activity of highly porous ZnO thin films prepared by sol–gel process, *Materials Chemistry and Physics*, 76 (2002) 82–87.

[17] K.Y. Jung, Y.C. Kang, S.B. Park, Photodegradation of trichloroethyleneusing nanometre-sized ZnO particles prepared by spray pyrolysis, *Journal of Materials Science Letters*, 16 (1997) 1848–1849.

[18] R. Wang, J.H. Xin, Y. Yang, H. Liu, L. Xu, J. Hu, The characteristics and photo catalytic activities of silver-doped ZnO nanocrystallites, *Applied Surface Science*, 227 (2004) 312–317.

[19] K. Vanhesuden, W.L. Warren, J.A. Voigt, C.H. Seager, D.R. Tallant, Impact of Pb doping on the optical and electronic properties of ZnO powders, *Applied Physics Letters*, 67 (1995) 1280–1282.

[20] S. Colis, H. Bieber, S. Begin-Colin, G. Schmerber, C. Leuvrey, A. Dinia, Magnetic properties of Co-doped ZnO diluted magnetic semiconductors prepared by low-temperature mechano synthesis, *Chemical Physics Letters,* 422 (2006) 529–533.

[21] C.P. Sibu, S.R. Kumar, P. Mukundan, K.G.K. Warrier, Structural Modifications and Associated Properties of Lanthanum Oxide Doped Sol−Gel Nanosized Titanium Oxide, *Chemistry of Materials*, 14 (2002) 2876-2881.

[22] S.C. Padmanabhan, S.C. Pillai, J. Colreavy, S. Balakrishnan, D.E. McCormack, T.S. Perova, Y. Gun'ko, S.J. Hinder, J.M. Kelly, Nanotechnology for environmental decontamination, *Chemistry of Materials*, 19 (2007) 4474-4481.

[23] V. Subramanian, E. Wolf, P.V. Kamat, Semiconductor−Metal Composite Nanostructures. To What Extent Do Metal Nanoparticles Improve the Photocatalytic Activity of TiO_2 Films?, *Journal of Physical Chemistry B*, 105 (2001) 11439-11446.

[24] S.C. Pillai, P. Periyat, R. George, D. McCormack, M.K. Seery, H. Hayden, J. Colreavy, D. Corr, S.J. Hinder, Synthesis of high temperature stable anatase TiO_2 photocatalyst, *Journal of Physical Chemistry C*, 111 (2007) 1605-1611.

[25] R. Asahi, T. Morikawa, T. Ohwaki, K. Aoki, Y. Taga, Visible-light photocatalysis in nitrogen-doped titanium oxides, *Science*, 13 (2001) 269-271.

[26] X. Qiu, G. Li, X. Sun, L. Li, X. Fu, Doping effects of Co(2+) ions on ZnO nanorods and their photocatalytic properties, *Nanotechnology*, 19 (2008) 215703.

[27] H.M. Zhou, D.Q. Yi, Z.M. Yu, L.R. Xiao, Jian Li, Preparation of aluminum doped zinc oxide films and the study of their microstructure, electrical and optical properties, *Thin Solid Films*, 515 (2007) 6909-6914.

[28] S. Ekambarama, Y. Iikubo A. Kudo, Combustion synthesis and photocatalytic properties of transition metal-incorporated ZnO, Journal of Alloys and Compounds. 433 (2007) 237-240.

[29] T.H. Ko, H. Chub, Y.J. Liou, A study of Zn–Mn based sorbent for the high-temperature removal of H_2S from coal-derived gas, *Journal of Hazardous Materials*, 147 (2007) 334-341.

[30] [30] T. Pauporte, J. Rathousky, Electrodeposited Mesoporous ZnO Thin Films as Efficient Photocatalysts for the Degradation of Dye Pollutants, *Journal of Physical Chemistry C*, 111 (2007) 7639-7644.

[31] R. L. Qiu, D.D. Zhang, Y. Q. Mo, L. Song, E. Brewer, X.F. Huang, Y. Xiong, Photocatalytic activity of polymer modified ZnO under visible light irradiation, J*ournal of Hazardous Materials*, 156 (2008) 80-85.

[32] F.D. Mai, C.C. Chen, J.L. Chen, S.C. Liu, Photodegradation of methyl green using visible irradiation in ZnO suspensions: determination of the reaction pathway and identification of intermediates by a high-performance liquid chromatography-photodiode array-electro spray ionization-mass spectrometry method, *Journal of Chromatography A*, 1189 **(**2008**)** 355-65.

[33] T.Q. Liu, O. Sakurai, N. Mizutani, M. Kato, Preparation of spherical fine ZnO particles by the spray pyrolysis method using ultrasonic atomization techniques, *Journal of Materials Science*, 21 (1986) 3698-3702.

[34] T. Trindade, J.D. Pedrosa Jesus, P. O'Brien, Preparation of zinc oxide and zinc sulfide powders by controlled precipitation from aqueous solution, *Journal of Materials Chemistry*, 4 **(**1994**)** 1611-1617.

[35] M.A. Verges, M.M. Gallego, Spherical and rod-like zinc oxide microcrystals: morphological characterization and micro structural evolution with temperature, *Journal of Materials Science*, 27 **(**1992**)** 3756-3762.

[36] D. Chen, X. Jiao, G. Cheng, Hydrothermal Synthesis of Zinc Oxide Powders with Different Morphologies, *Solid State Communications*, 113 (2000) 363-366.

[37] S. Mahamuni, K. Borgohain, B.S. Bendre, J.L. Valene, H.R. Subhash, Spectroscopic and structural characterization of electrochemically grown ZnO quantum dots, *Journal of Applied Physics*, 85 (1999) 2861-2865.

[38] E. Bulut, M. Ozacar, Adsorption of malachite green onto bentonite: equilibrium and kinetic study and process design, *Microporous Mesoporous Materials*, 115 (2008) 234–246.

[39] E. Evgenidou, K. Fytianos, I. Poulios, Semiconductor-sensitized photodegradation of dichlorvos in water using TiO_2 and ZnO as catalysts, *Applied Catalysis B: Environmental*, 59 (2005) 81-89.

[40] A.C. Tas, P.J. Majewski, F. Aldinger, Chemical preparation of pure and strontium- and/or magnesium-doped lanthanum gallate powders, *Journal of the American Ceramic Society*, 83 (2000) 2954-2960.

[41] K.M. Reddy, S.V. Panorama, A.R. Reddy, Bandgap studies on anatase titanium dioxide nanoparticles, *Materials Chemistry and Physics*, 78 (2003) 239–245.

[42] [42] M. Bitenc, M. Marinsek, Z.C. Orelm, Preparation and characterization of zinc hydroxide carbonate and porous zinc oxide particles, *Journal of the European Ceramic Society,* 28 (2008) 2915–2921.

[43] G. Marci, V. Augugliaro, M.J. Lopez-Munoz, C. Martin, L. Palmisano, V. Rives, M. Schiavello, R.J.D. Tilley, A.M. Venezia, Preparation Characterization and Photocatalytic Activity of Polycrystalline ZnO/TiO_2 Systems. 2. Surface, Bulk Characterization, and 4-Nitrophenol Photodegradation in Liquid−Solid Regime, *Journal of Physical Chemistry B*, 105 (2001) 1033–1040.

[44] K. Mehrotra, G.S. Yablonsky, A.K. Ray, Kinetic Studies of Photocatalytic Degradation in a TiO_2 Slurry System: Distinguishing Working Regimes and Determining Rate Dependences, *Industrial & Engineering Chemistry Research*, 42 (2003) 2273–2281.

[45] J.B. De Heredia, J. Torregrosa, J.R. Dominguez, J.A. Peres, Oxidation of p-hydroxy benzoic acid by UV radiation and by TiO_2/UV radiation: comparison and modelling of reaction kinetic, *Journal of Hazardous Materials*, 83**(**2001**)** 255–264.

[46] I. Poulios, I. Tsachpinis, Photodegradation of the textile dye Reactive Black 5 in the presence of semiconducting oxides, *Journal of Chemical Technology & Biotechnology*, 74 (1999) 349.

[47] I. Poulios, I. Aetopoulou, Photocatalytic Degradation of the Textile Dye Reactive Orange 16 in the Presence of TiO_2 Suspensions, *Environmental Technology*, 20 **(**1999**)** 479-487.

[48] N. San, A. Hatipoglu, G. Kocturk, Z. Cinar, Prediction of primary intermediates and the photodegradation kinetics of 3-aminophenol in aqueous TiO_2 suspensions, *Journal of Photochemistry and Photobiology A: Chemistry*, 139 (2001) 225-232.

[49] A. Mills, R.H. Davis, D. Worsely, Water-purification by semiconductor photocatalysis, *Chemical Society Reviews*, 22 (1993) 417-425.

[50] I. Arslan, I.A. Balcioglu, T. Tuhkanen, Advanced Oxidation of Synthetic Dyehouse Effluent by O_3, H_2O_2/O_3 and H_2O_2/UV Processes, *Environmental Technology*, 20 **(**1999**)** 921-931.

[51] W.Z. Tang, H. An, Photocatalytic Degradation Kinetics and Mechanism of Acid Blue 40 by TiO_2 UV in Aqueous Solution, *Chemosphere*, 31 (1995**)** 4171-4183.

[52] D. Nansheng, F. Tao, T. Shizhong, Photodegradation of dyes in aqueous solutions containing Fe(II)-hydroxy complex I. Photodegradation kinetics, *Chemosphere*, 33 (1996) 547-557.

[53] L. Wenhua, L. Hong, C. Suo'an, Z. Jianqing, C. Chunan, Kinetics of photocatalytic degradation of aniline in water over TiO_2 supported on porous nickel, *Journal of Photochemistry and Photobiology A: Chemistry*, 131 (2000) 125-132.

[54] M. Abdullah, G.K.C. Low, R.W. Matthews, Effects of common inorganic anions on rates of photocatalytic oxidation of organic carbon over illuminated titanium dioxide, *Journal of Physical Chemistry*, 94 (1990) 6820-6825.

[55] G. Thennarasu, A. Sivasamy, Enhanced visible photocatalytic activity of cotton ball like nano structured Cu doped ZnO for the degradation of organic pollutant, *Ecotoxicology and Environmental Safety*, 134 (2016) 412-420.

[56] G. Thennarasu, A. Sivasamy, Metal ion doped semiconductor metal oxide nanosphere particles prepared by soft chemical method and its visible light photocatalytic activity in degradation of phenol, *Powder Technology*, 250 (2013), 1-12.

Acknowledgement

This research received no specific grant from any funding agency in the public, commercial, or not-for-profit sectors.

Competing Interests:

The authors declare that they have no competing interests.

About The License